A. Kamath
(GE Global Research Centre)

P. P. Menon
(College of Engineering, Mathematics and Physical Sciences, University of Exeter)

M. Ganet-Schoeller, G. Maurice
(Ariane Group)

S. Bennani
(Guidance, Navigation and Control Section, ESA/ESTEC)

E-mail: p.m.prathyush@exeter.ac.uk

DOI: 10.12762/2017.AL13-09

Surrogate Assisted Computation of the Parametric Safety Margin for a Flexible Launcher

In order to assess the robustness of dynamical systems, an approach is to demarcate the uncertain parameter space as safe set and unsafe set. Unsafe set represents the region within which the system lacks the required level of performance, or even loses its stability. However, determining the minimum distance metric for the unsafe set from the nominal operating point, the so-called parametric safety margin, for a higher dimensional dynamical system is not trivial and is often computationally demanding. In this paper, the parametric safety margin for a closed loop industrial standard launch vehicle simulator during its thrust vector control phase is computed. Imposing certain basic topological restrictions for the multi-dimensional uncertain parameter space, the computation of the parametric safety margin can be posed as a constrained non-convex global optimization problem, and is thus extremely challenging in the case of high-fidelity aerospace simulators. Various performance requirements become the constraints in the optimization problem. An approach exploiting the use of non-intrusive polynomial surrogate modeling is proposed for the efficient computation of the parametric safety margin for the industrial standard launch vehicle simulator.

Introduction

In order to ensure the safety of a space mission, the controller needs to ensure robust stability and performance in the presence of various uncertainties and disturbances[1]. Uncertainties emanating from the mission parameters, such as aero-thermodynamic parameters, physical configuration parameters such as mass, inertia, actuator and sensor uncertain parameters, and flexible mode parameters, are to be considered. During the design cycle [2], the performance of the controller is assessed using a range of methods, such as analytical techniques that could be employed on lower order models, simulation-based techniques that are applicable to more detailed, complex and high-fidelity models [3], hardware in loop analysis, where actual subsystems replace some of the mathematical models [4] and the flight tests [5]. Analytical techniques, such as gain/phase margins [6] and the nonlinear continuation/bifurcation analysis against single parameter variations [7] can be considered as the traditional analytical tools for worst-case analysis in the early phase of the design cycle. Multivariable methodologies, such as μ-analysis and ν-gap metric analysis (Chapters 17 and 18, of Ref. [1]) became modern candidates for carrying out worst-case analysis based on a robust control theory, representing a given closed-loop system in a Linear Fractional Transformation (LFT)-based representation ([8] and Chapter 3, 4 and 5 of Ref. [9]). These techniques and their variants deal with multiple sources of uncertainty; however, the complexity in determining the exact μ value is claimed to be an NP-hard problem [10] and an excellent bound comparison using several variants of the algorithm on various benchmark problems can be found in [11]. Useful extensions of these approaches, which can handle certain types of nonlinear dynamics, have also recently been developed, such as Integral Quadratic Constraints (IQC)([12, 13] and Chapter 10 of Ref. [9]) and Sum Of Squares (SOS) programming [14].

The key advantages, as well as the conservatism and the limitations from the perspective of the requirements of the underlying uncertain model for many of these analytical methods, can be found in the conclusions of Chapter 3, 4, 5 and 10 of Ref [9]. Sampling and simulation-based analysis techniques, such as Monte Carlo and optimization methods, have specific advantages when dealing with nonlinear and complex models. Determining the worst case perturbations that lead to large excursions of the desired design metrics can be formulated as maximization problems and can be solved using various optimization algorithms [3, 1, 15, 16, 17, 9]. Despite the common generic mathematical formulation of the maximization problem, the quality of the worst-case solution and the computational complexity depend on the underlying methods selected for the

analysis. However, relatively fewer limitations are imposed on the requirements of the closed-loop mathematical models. That said, the computational time required for each simulation can possibly impose restrictions, if excessive. In that case, one would be forced to limit their analysis based on the available computational budget, or depend on other surrogate modeling techniques.

Parametric safety margin metric estimation provides another method (based on a simulation and optimization-based analysis concept) to assess the robustness of the controller [18]. This metric is defined in the parameter space as the distance between the nominal parameter value and the parameter value that corresponds to the first violation instance of a performance criterion. The implementation of this method on an aerospace benchmark with a complex nonlinear model is computationally challenging. When dealing with highly complex nonlinear models, a single function evaluation might take several seconds, which when used in an optimizer can take several hours until a global optimum is reached. The computation requirement for the parametric safety margin may benefit from the use of surrogate models instead of the actual full-order model. The use of surrogate models to evaluate the parametric safety margin will give the control system designer an estimate of the robustness of the designed controller within a matter of minutes. The designer can then evaluate the full-order model only in the zone of interest to check the validity of the parametric safety margin. Although in the literature there are plethora of methods available to build surrogate models,[19, 20, 21, 22, 23], to name a few. This paper focuses on the use of the polynomial chaos methodology, since it utilizes a limited number of input configurations to derive a surrogate model. In order to avoid large computation times to evaluate the complex nonlinear model, a surrogate model is developed using just a minimal number of evaluations of the original model, without compromising on accuracy as per the polynomial chaos methodology. Such a surrogate model provides an approximation to the simulator for any input configurations, and hence may be used to replace the original simulator for the fast computation of responses. The contribution of this paper is in the application of three different schemes, such as the parametric safety margin method, surrogate modeling using polynomial chaos, and optimization-based worst case analysis, which are integrated with the analysis of a flexible launcher model.

This paper is organized as follows: at first, the problem definition is provided. The description of the launcher model along with its functional performance criteria is given in Section "Closed-Loop System Description". A brief description of the theory of parametric safety margin estimation and the surrogate polynomial model is provided in Section "Analysis Methods". Section "Main Results" presents the results of the parametric safety margin with launcher, as well as polynomial models. Finally, a worst-case analysis is performed, in order to ascertain the maximum deviations of the performance criteria.

Problem Definition

A closed-loop dynamical system representation of a flexible launcher is provided, and the control law design is carried out to meet a set of mission performance objectives in a robust manner. The given model is treated as a "black-box" with access limited to certain input and output parameters, as is often the case with many other industrial models that are used for the purpose of validating and verifying the controllers. Given a bounded, multi-dimensional uncertain space, $\Delta \subset \mathcal{R}^m$, the questions that we are trying to answer are the following:

- Determine an operational parametric safety margin; *i.e.*, the set within which all different mission performance objectives associated with the closed-loop design are satisfied.
- Determine the combination of uncertain parameters associated with a maximum possible violation of a mission performance objective, $\delta^* \in \Delta \subset \mathcal{R}^m$, which is identified as the worst-case perturbation.
- Address computational complexities due to the time consuming simulations, while determining the parametric safety margin, by replacing the actual closed-loop dynamics model with its representative meta/surrogate model.

A constrained optimization problem is employed, in order to determine the parametric safety margin. The closed-loop functional performance requirements are written as a set of inequality constraints $\mathbf{s}(\delta, \mathcal{C}_{\mathcal{H}_\infty}, W) < 0$, where $\mathcal{C}_{\mathcal{H}_\infty}$ is the class of control law used and W is the wind gust disturbance profile and $\delta \in \Delta \subset \mathbb{R}^{dim(\delta)}$. The closed-loop design is said to be robust and acceptable if all of the constraints $\mathbf{s}(\delta, \mathcal{C}_{\mathcal{H}_\infty}, W) < 0$ are satisfied in the presence of various combinations of uncertain parameter perturbations.

The uncertain parameter space (Δ - space) can be classified as a safe or unsafe region, depending on whether the constraints $\mathbf{s}(\delta, \mathcal{C}_{\mathcal{H}_\infty}, W) < 0$ are satisfied or not, respectively. The unsafe region, denoted as $\mathcal{S}^u(\mathbf{s}) \subset \mathbb{R}^{dim(\delta)}$, is given by

$$\mathcal{S}^u(\mathbf{s}) = \bigcup_{i=1}^{dim(\mathbf{s})} \mathcal{S}_i^u(\mathbf{s})$$

where, for $1 \le i \le dim(\mathbf{s})$,

$$\mathcal{S}_i^u(\mathbf{s}) = \left\{ \delta \in \mathbb{R}^{dim(\delta)} : \mathbf{s}_i\left(\delta, \mathcal{C}_{\mathcal{H}_\infty}, W\right) > 0 \right\}$$

$\mathcal{S}^u(\mathbf{s})$ is the union of all unsafe regions defined by the individual constraints. The boundary of the set is on $\mathbf{s}(\delta, \mathcal{C}_{\mathcal{H}_\infty}, W) = 0$. The complementary set $\mathcal{S}'^u(\mathbf{s})$ becomes the safe set. At least one constraint must be violated in the unsafe region, while in the safe region all of the performance constraints are satisfied.

The method involves the definition of a reference set in the parameter space, with the nominal parameter vector δ_0 as the geometric center. This reference set is then subjected to homothetic dilations (*i.e.*, expansion and contraction) until the first instance of violation of the constraints $\mathbf{s} < 0$ occurs. In other words, we are interested in evaluating the largest safe set, $\mathcal{S}'^u(\mathbf{s})$, around the nominal parameter value. The size of this set is directly related to the operational uncertainty margin. Further details on the evaluation of the operational uncertainty margin can be found in Section "Analysis Methods".

The evaluation of the operational uncertainty margin becomes computationally very expensive when applying it to an industry standard problem. Given that performance criteria are treated as constraints, a closed-loop dynamical system is simulated and performance criteria are evaluated in the constraint function of the optimization scheme. Since the dynamical system is evaluated in the constraint function, the process of evaluating the operational uncertainty margin becomes computationally expensive. Identifying the exact operational

uncertainty margin, which may be a non-convex multidimensional surface, or even disconnected regions, with an attractive and feasible computational effort is challenging. Hence, an approximate operational margin that could be conservative, yet determined with a reduced computational effort, is preferred.

Computational effort could be considerably reduced if the constraint function were in polynomial form. Hence, a polynomial model is preferred instead of a closed-loop dynamical model. However, depending on the accuracy of the polynomial model, the safety margin could be optimistic or conservative. A conservative margin will always be safe, but optimistic safety margins may contain regions of the parametric space where constraints are violated. In order to be absolutely sure that the uncertainty margin truly contains no constraint violation, we perform a worst-case analysis on the reduced region defined by the margin. If no worst cases are found inside this region, then the margin is valid.

Closed-Loop System Description

Launcher Model and Control

A single-axis, parameter-varying model [24], derived by linearization of complete non-linear dynamic equations of motion for a flexible launcher under various equilibrium flight conditions, is considered as the benchmark for this study. A H_∞ controller is provided for the pitch control of the launcher during the atmospheric flight phase, from take-off to tail-off [24]. Rigid and bending mode dynamics together with an actuator, bending mode filter and H_∞ controller are modeled and implemented in MATLAB R2008b Simulink. The rigid-body dynamics during the atmospheric flight phase are described by the following three state representations:

$$\begin{bmatrix} \ddot{\theta} \\ \dot{\theta} \\ \ddot{Z} \end{bmatrix} = \begin{bmatrix} 0 & A_6(t) & A_6(t)/V(t) \\ 1 & 0 & 0 \\ 0 & A_1(t) & -A_6(t)\alpha_3(t) \end{bmatrix} \begin{bmatrix} \dot{\theta} \\ \theta \\ \dot{Z} \end{bmatrix} + \begin{bmatrix} K_1(t) & -A_6(t)/V(t) \\ 0 & 0 \\ K_2(t) & A_6(t)\alpha_3(t) \end{bmatrix} \begin{bmatrix} \beta \\ W \end{bmatrix} \quad (1)$$

In which parameters such as aerodynamic efficiency $A_6(t)$, aerodynamic coefficient $A_1(t)$, aero thruster efficiency $K_1(t)$ and $K_2(t)$, and $\alpha_3(t)$ are time-varying along the trajectory and are defined as follows [24]:

$$A_1 = -\frac{P_C + P_S}{m} + \frac{QS_{ref}}{m}\left(C_A - C_{N\alpha}\right)$$

$$A_6 = \frac{QS_{ref} C_{N\alpha} L_F}{I}$$

$$K_1 = \frac{P_C l_{tu}}{I} \qquad K_2 = -\frac{P_C}{m} \qquad \alpha_3 = \frac{I}{m(t)V} L_F$$

In (1), $Col(\dot{\theta}, \theta, \dot{Z})$ are states of the rigid mode dynamics and correspond to the launcher pitch rate (deg/sec), pitch angle (deg) and drift velocity (m/s) in the body frame, respectively. β and W represent the control input deflections and the wind perturbation, respectively. In the definitions of the aerodynamic and thruster efficiency parameters $A_i(t)$ and $K_i(t)$: $V, P_C, P_S, Q, S_{ref}, C_A, C_{N\alpha}, L_F, l_{tu}, I$ and m represent the absolute velocity, commanded thrust level, thrust level along the longitudinal axis, dynamic pressure, reference area, axial force coefficient, normal aerodynamic force coefficient with respect to the angle of attack, distance between the center of gravity and center of pressure on longitudinal axis, position of nozzle rotation with respect to the center of gravity, total inertia and total mass, respectively.

A second-order model with a small damping value represents the flexible bending mode dynamics associated with the flexible launcher, and is modeled as an additive perturbation on the rigid-body model. The flexible mode dynamics are represented as follows [24]:

$$\ddot{q}_i + 2\xi_i\omega_i\dot{q}_i + \omega_i^2 q_i = -P_C h_{tu_i}\beta_C + \left(I_T h_{ptu_i} - M_{tu} L_{tu}\left(h_{tu_i} - L_{tu} h_{ptu_i}\right)\right)\ddot{\beta}_C \quad (2)$$

where q_i, ξ_i, ω_i, h_{tu_i}, I_T, h_{ptu_i}, M_{tu}, L_{tu} and β_C represent the ith bending mode state, i^{th} bending mode damping, i^{th} bending mode pulsation, i^{th} bending mode deformation at the nozzle rotation point, total pitch inertia, i^{th} bending mode slide of deformation at the nozzle rotation point, nozzle mass, position of nozzle CoG respective to the nozzle rotation point and the commanded deflections around the nominal value to follow the reference trajectory. A total of five bending modes are considered in this benchmark. The actuator model for the pitch control is characterized by a second-order system having commanded deflection as a single input, and the realized deflection and its two derivatives as the three outputs.

$$\ddot{\beta}_R + 2\xi_\beta\omega_\beta\dot{\beta}_R + \omega_\beta^2\beta_R = \omega_\beta^2\beta_C \quad (3)$$

where, ξ_β and ω_β represent the damping of the actuator model and the actuator model pulsation. The final effective deflection angle β corresponds to the sum of the realized control input deflection (β_R) and the misalignment deflection (β_{FZ}), and is given as:

$$\beta = \beta_R + \beta_{FZ} \quad (4)$$

The pitch angle is derived from the attitude measurement by the Inertial Measurement Unit (IMU) and the pitch rate is derived from the angular rate measurement by the gyrometer. hp_{IMUi} is the ith bending mode slide of deformation at the IMU location and hp_{GYi} is the ith bending mode slide of deformation at the gyrometer location. Noises are added to these measurements. Angular noise and angular rate noises are treated as Gaussian with 0.02° and 0.15°/s standard deviation, respectively.

$$\theta_m = \theta - \sum_i hp_{IMUi} q_i + noises$$
$$\dot{\theta}_m = \dot{\theta} - \sum_i hp_{GYi}\dot{q}_i + noises \quad (5)$$

A discrete time-robust gain-scheduled controller is used with the benchmark model (see the block interconnection in Figure 1), which consists of an H_∞ rigid-mode controller and a filter, which is kept in

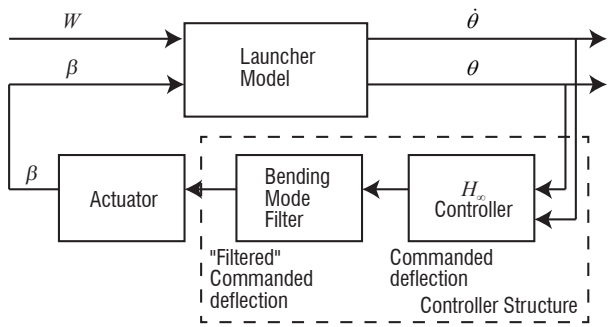

Figure 1 – Block description of the flexible launcher vehicle

series with the controller, for robust attenuation of the bending modes. The angular position and rate are the inputs of the controller and the filtered commanded deflection is the output. Further details on the model can be found in [24, 25].

Disturbances

The external disturbance corresponds to the wind gradient and the wind gust. The wind gust is a sudden increase/decrease in wind speed. This wind disturbance is assumed to be applied at the center of gravity of the flexible launcher vehicle. In this study, the wind perturbation is modeled by synthetic wind from a wind envelope, wind shear (wind speed change divided by the altitude interval) and wind gust according to a NASA specification in [26]. Synthetic wind is commonly used by aerospace organizations for vehicle design computations. Wind envelope and wind shear both come from wind measurements collected at the area of interest over a long period, and wind gust is an arbitrary characterization of the small scale motion. The NASA database given in [26] is followed. The synthetic wind is determined by an altitude, which corresponds to the maximum wind gradient. It is also the altitude at which the wind takes the value of the envelope. In this tool, the input is a flight instant and altitude is computed from the trajectory data using this instant. We have considered a deterministic wind profile occurring at five flight instances, 30, 35, 40, 45 and 50 seconds, as shown in Figure 2. Wind disturbance occurring early on in the flight interval can make the vehicle unstable and, hence, focus is on five instances between 30 to 50 seconds. Other wind instances were also considered during the analysis, but not reported here because they did not have any significant impact on the launch vehicle.

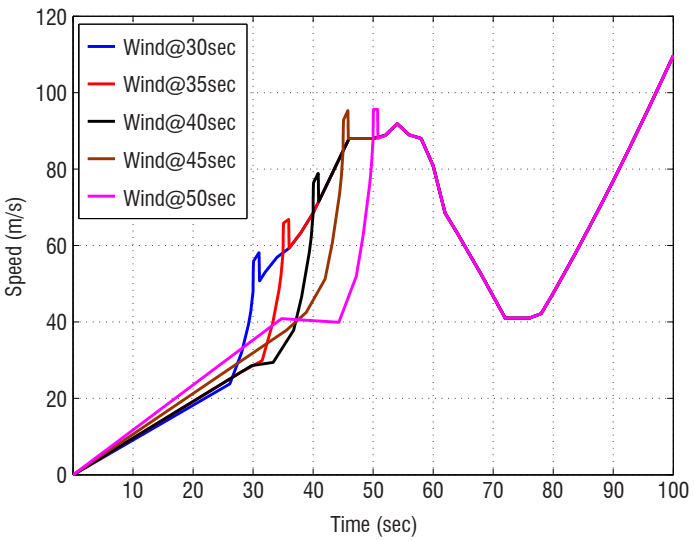

Figure 2 – Wind Profile

Uncertainties

For the given launcher controller/payload configuration, twenty eight uncertainties are considered in this study, which constitute eight rigid-mode parameters and five bending-mode parameters (i^{th} bending-mode pulsation, deformation at the nozzle position, slide deformation at the nozzle location, slide deformation at the IMU location and slide deformation at the gyrometer location), with four bending modes each, are considered. The entire list of uncertainties is given in Table 1. The uncertainty domain consists of two aspects: a possible nominal domain, which is not well-known prior to the flight, but can be known and reduced after the qualifications of the flights (reducible uncertainty) and, secondly, a dispersion domain in which the parameter value can change from one mission to another. In the framework of worst-case analysis, bounds on uncertain parameters are utilized by optimization tools to generate the worst case. These bounds should be able to incorporate both the uncertainties and the dispersions associated with the parameters. Such types of bounds were defined by ASTRIUM and the CNES for launcher application, as presented in [27], and are used in this study.

	Parameters	Uncertainty	Dispersion
Rigid	Inertia (MI)	±10%	±3%
	Thrust (MP)	±3%	±1%
	Aerodynamic coefficient(MCz)	±20%	±10%
	Centre of pressure (MXf)	±1.79 m	±0.2 m
	Dynamic pressure (MQ)	±20%	±4%
	Centre of gravity (MXg)	±0.3 m	±0.05 m
	Mass (MM)	5%	–
	Deflection Misalignment ($\Delta\beta$)	1°	–
Bending mode	Pulsation ($Mpuls$)	±20%	–
	Deformation at the nozzle location ($Mhtu$)	±30%	–
	Slide deformation at the nozzle location ($Mhptu$)	±30%	–
	Slide deformation at IMU location ($MhpIMU$)	±30%	–
	Slide deformation at the Gyrometer location ($MhpIMU$)	±30%	–

Table 1 – Variability of rigid and bending-mode uncertain parameters

Specifications

The controller structure ($\mathcal{C}_{H_\infty}$), consisting of the H_∞ controller and the bending-mode filter, must satisfy various functional performance requirements during the atmospheric phase control. The main functional requirements are the compensation for external wind and wind gust perturbations, and compensation for the internal perturbations, which include the thrust misalignment, the static error of the servo-actuators and thrust asymmetry. The compensation scheme must maintain minimum aerodynamic loads (Q_α, which is the angle of attack times the dynamic pressure), for structural sizing reasons. The main temporal performance specifications that are to be validated and the margins to be assessed, in the presence of multiple uncertain parameter perturbations and dispersions, are listed in Table 2.

Specification Description	Requirement	Cost function
$s_1(.)$: Maximum value of the aerodynamic angle of attack ($Q_\alpha(t)$) compatible with general load specification simulated over a finite time period	$< 500\ kPadeg$	$\max_{t\in[t_0 t_f]} \lvert Q_\alpha(t)\rvert$
$s_2(.)$: Maximum final value of the attitude ($\theta(t_f)$)	≤ 2°	$\max \lvert\theta(t_f)\rvert$
$s_3(.)$: Maximum final value of the attitude rate ($\dot{\theta}(t_f)$)	≤ 0.8°/s	$\max \lvert\dot{\theta}(t_f)\rvert$
$s_4(.)$: Maximum value of the deflection angle ($\beta(t)$) simulated over a finite time period	< 6°	$\max_{t\in[t_0 t_f]} \lvert\beta(t)\rvert$
$s_5(.)$: Cumulative deflection over a finite time period	< 200°	$\max \sum_{t_0}^{t_f} \lvert\Delta\beta_C\rvert$

Table 2 – Functional performance requirements

Analysis Methods

Parametric Safety Margin Assessment

The parameter space, $\Delta \subset \mathbb{R}^{dim(\delta)}$ can be divided into safe and unsafe regions, where the safe region corresponds to a region where all of the functional performance criteria are satisfied and the unsafe region corresponds to a region where at least one of the functional performance criteria is violated.

In this study, the chosen reference set, $\mathcal{M} \subset \Delta := \delta \in [\delta_{min}, \delta_{max}]$, is assumed to be a hyper rectangle with each component of the uncertain parameter vector, $\delta \in \mathbb{R}^{dim(\delta)}$, defined over a bounded interval. Assume symmetry around the geometric center, which corresponds to the nominal parameter value (δ_0). Let $\mathbf{m}$ be the vector of half-lengths of the sides of the hyper-rectangle. The hyper-rectangle $\mathcal{R}(\delta_0, \mathbf{m})$ is defined as

$$\mathcal{R}(\delta_0, \mathbf{m}) := \left\{ \delta \mid \delta^i \in [\delta_0^i - \mathbf{m}^i, \delta_0^i + \mathbf{m}^i], 1 \le i \le dim(\delta) \right\} \tag{6}$$

$\mathcal{R}(\delta_0, \mathbf{m})$ is called the reference set, which is chosen by selecting the values of the vector of half-lengths $\mathbf{m}$. This reference set, $\mathcal{R}(\delta_0, \mathbf{m})$, is depicted by a dashed blue line in Figures 3(a) and 3(b). A homothetic scaling of the reference set by a scaling factor λ is $\mathcal{R}(\delta_0, \lambda\mathbf{m}) := \{\delta_0 + \lambda(\delta - \delta_0) \mid \delta \in \mathcal{R}(\delta_0, \mathbf{m})\}$. Suppose that λ is positive; the resultant set is expanded with respect to the reference set, in Eq. 6 and if λ is negative, the resultant set is contracted with respect to the reference set in Eq. 6. The ratio of expansion or contraction is called the similitude ratio, $\lambda \in \mathbb{R}$. The similitude ratio is a positive scaling factor. The similitude ratio condition $\lambda > 1$ corresponds to the expansion, and the similitude ratio in the range of $0 < \lambda < 1$ corresponds to the contraction of the reference set, $\mathcal{R}(\delta_0, \mathbf{m})$. By successive dilations of the reference set, *i.e.*, expansions and contractions, the objective is to determine the largest safe set, $\mathcal{S}'^u(\mathbf{s})$, around the nominal parameter value. The largest set is depicted by the red line in Figures 3(a) and 3(b) and is represented as $\mathcal{R}(\delta_0, \tilde{\lambda}\mathbf{m})$, where $\tilde{\lambda}$ is called the critical similitude ratio. The critical similitude ratio is a non-dimensional positive scaling value denoted as $\tilde{\lambda}$. It is the similitude ratio of the dilation, and is interpreted as the operational parametric safety margin, ρ, for satisfaction of all of the functional performance requirements in the parameter space. The corresponding uncertain parameter combination is termed as a critical parameter vector. Hence, although conservative, this would be viewed as the onset of a violation of at least one performance criterion in the certain parameter space. There could be certain directions in which an expansion might still be possible, depending on the complex topology of the safe uncertainty set.

The sets $\mathcal{R}(\delta_0, \mathbf{m})$ and the scaled set $\mathcal{R}(\delta_0, \tilde{\lambda}\mathbf{m})$ are proportional. In Figure 2, the reference set, $\mathcal{R}(\delta_0, \mathbf{m})$ has expanded to $\mathcal{R}(\delta_0, \tilde{\lambda}\mathbf{m})$, which implies that the unsafe region $\mathcal{S}^u$ is outside the reference set. Whereas in Figure 2, the reference set $\mathcal{R}(\delta_0, \mathbf{m})$ has contracted to $\mathcal{R}(\delta_0, \tilde{\lambda}\mathbf{m})$, implying that the unsafe region is inside the reference set. Naturally, good robustness is associated with the expansion of the reference set, whereas the contraction implies poor robustness, since even a small perturbation around the nominal parameter value would result in violation of performance criteria. This is a measure of robustness of the controller, $\mathcal{C}_{\mathcal{H}_\infty}$, implying how large an uncertain parameter set can be to be identified as safe with respect to the nominal point. The constraint $\mathbf{s}(\delta, \mathcal{C}_{\mathcal{H}_\infty}, W)$ might have a nonlinear dependency on the parameters, and hence the computation of the critical parameter value becomes a non-convex global optimization problem. Furthermore, for the purpose of checking the satisfaction of the constraints, a simulation of the closed-loop model and the evaluation of each performance constraint is required.

The critical parameter value corresponding to the dilation of the reference set $\mathcal{R}(\delta_0, \mathbf{m})$ in the case of the ith constraint can be computed by solving

$$\tilde{\delta}^i = \underset{\delta}{arg\,min} \left\{ \|\delta - \delta_0\|_{\mathbf{m}}^{\infty} \mid \mathbf{s}_i\left(\delta, \mathcal{C}_{\mathcal{H}_\infty}, W\right) \ge 0 \right\} \tag{7}$$

where $\|\delta - \delta_0\|_{\mathbf{m}}^{\infty} := \underset{i}{arg\,sup} \left\{ \frac{|\delta - \delta_0|_i}{\mathbf{m}_i} \right\}$, is the $\mathbf{m}$-scaled norm. Considering all of the performances, the overall critical parameter value is $\tilde{\delta} = \tilde{\delta}_k$, where $k = \underset{1 \le j \le dim\delta}{arg\,min} \left\{ \|\tilde{\delta}_j^i - \delta_0\|_{\mathbf{m}}^{\infty} \right\}$, which is associated with the critical requirement. The resultant set $\mathcal{R}(\delta_0, \tilde{\lambda}\mathbf{m})$ is proportional to $\mathcal{R}(\delta_0, \mathbf{m})$, where $\tilde{\lambda} = \|\tilde{\delta} - \delta_0\|_{\mathbf{m}}^{\infty}$, in a non-dimensionalized setting.

The operational parametric safety margin is $\rho = \tilde{\lambda}\|\mathbf{m}\|$. The robustness is ensured when $\rho \ge \|\mathbf{m}\|$ for a given controller design. In such situation, all of the performance constraints $\mathbf{s}(\delta, \mathcal{C}_{H_\infty}, W) \le 0$ are

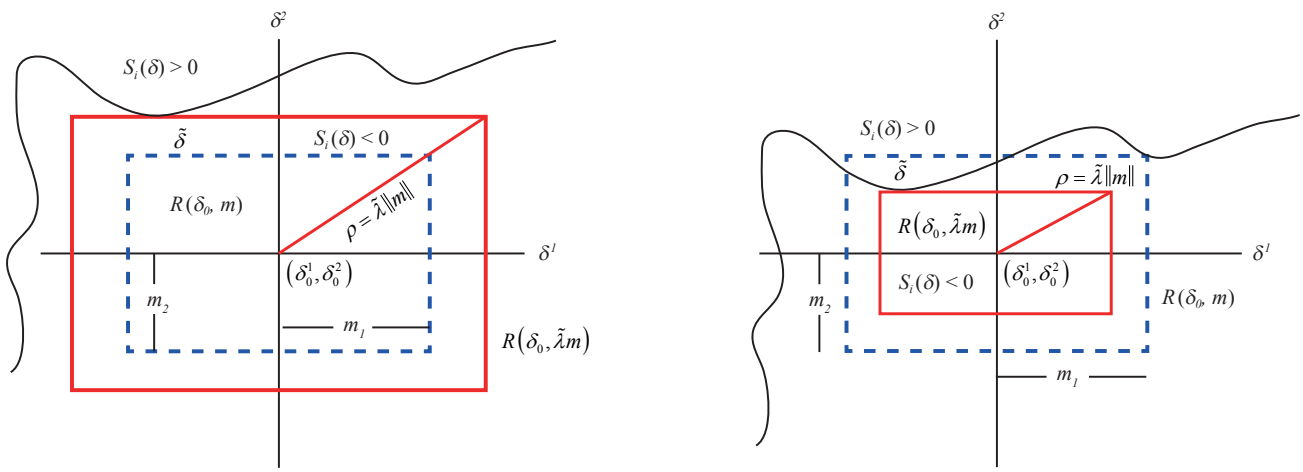

(a) Expansion

(b) Contraction

Figure 3 – Dilation of Uncertainty Set

satisfied in the region $\Delta = \mathcal{R}_\delta(\delta_0, \mathbf{m})$. Eq. 7 is reformulated as a constrained optimization problem, as follows:

$$\begin{aligned} \min \quad & \|\delta - \delta_0\|_{\mathbf{m}}^{\infty} \\ \text{Subject to:} \quad & \mathbf{s}_i\left(\delta, \mathcal{C}_{H_\infty}, W\right) \geq 0 \end{aligned} \tag{8}$$

where $\mathbf{s}_i(.)$ are the functional performance constraints listed in Table 2.

Surrogate assisted analysis

The evaluation of a parametric safety margin metric is computationally very expensive. Often, simulation-based optimization techniques,[18, 28, 29], can be computationally expensive and thus very time consuming. Further, the complexity of models can contribute to the time complexity. Here, we investigate the potential of surrogate polynomial models instead of the original launcher model, in order to save in terms of computational time overhead.

Polynomial models have been used in various applications, including solid mechanics [30, 31], stochastic finite elements [32] and stochastic fluid dynamics [33, 34]. In [35], power series expansion and polynomial chaos expansion are used to quantify the uncertainty in the output of nonlinear systems, and to illustrate it on a batch crystallization process. In [36], Polynomial Chaos is used to analyze the stability and control of a dynamical system with probabilistic uncertainty on the system parameters. Singh, [37], used the generalized polynomial chaos (gPC) method to design robust input shapers for precise control of mechanical systems. In aerospace applications, Fisher, [38], provided a framework based on gPC to analyze a linear flight-control design for an F-16 aircraft model.

The basic concept is to approximate the response of the model using a polynomial function of uncertain parameters. The polynomial function is constructed using an orthogonal polynomial basis ($\Phi_q(\delta)$). The underlying idea is as follows: the random variables, *i.e.*, various uncertain parameters to be perturbed, are represented as orthogonal functions of a stochastic variable with deterministic coefficients:

$$F = \sum_{q=0}^{\infty} a_q \Phi_q(\delta) \tag{9}$$

As shown in [39], a truncated version of the expansion ($q = 0, 1, \ldots, M$) is possible, where the order M depends on the number of uncertain parameters and the order of the polynomial sought.

$$F = \sum_{q=0}^{M} a_q \Phi_q(\delta) \tag{10}$$

where $M = \frac{(q_v + q_o)!}{(q_v! q_o!)} - 1$, q_v is the number of independent sources of uncertainty and q_o is the maximum order of the polynomial. Here, the coefficients a_q for $q = 0, \ldots, M$ have to be determined.

In [40], Wiener introduced homogeneous chaos for the Gaussian process, which utilized the span of the Hermite polynomial functionals to quantify uncertain parameters. This was later expanded to incorporate a non-Gaussian random process with polynomials from the Wiener-Askey scheme [39]. The connections between the choice of distribution and random variable, the Wiener-Askey polynomial and the support set are listed in Table 3. For example, for a continuous uniform distributed random variable, a Legendre polynomial basis with corresponding support set $[a, b]$ is selected.

	Random variable δ	Wiener-Askey Scheme	Support Set
Continuous	Gaussian	Hermite	$(-\infty, \infty)$
	Gamma	Laguerre	$[0, \infty)$
	Uniform	Legendre	$[a, b]$
	Beta	Jacobi	$[a, b]$

Table 3 – Wiener-Askey polynomials with corresponding distribution

The Galerkin projection method is generally used to evaluate the coefficients (a_q) in Eq. 10 [39, 38, 30]. This projection method involves solving multiple definite integrals, which could be computationally expensive and time-consuming in the presence of a large number of uncertain parameters. A non-intrusive method, called the probabilistic collocation method [41], is used to evaluate the coefficients (Φ_q) of the surrogate polynomial model. The model is treated as a "black box" type with access limited to a few uncertain input parameters and the output response. The method involves evaluation of the original model at specific selected points in the uncertain parameter space, identified as collocation points. The required number of collocation points also depends on the order of the polynomial and the number of uncertainties. The collocation points are chosen in such a way that the dynamical behavior of the original model should be captured as closely as possible. In order to do this, the collocation points are generated by evaluating the roots of the next higher-order polynomial in the orthogonal polynomial basis Φ_q. The pseudo-code for deriving the surrogate model is given as Algorithm 1 in [42].

Polynomial model of the Launcher

A polynomial model is derived by treating the flexible launcher model in a closed loop with the H_∞ controller as a black box, and considering the uncertain parameters as inputs and the cost function value as the output. In order to incorporate the effect of the noise acting on the outputs, the original Simulink model in MATLAB uses a random number generator. A seed value of the random number generator ensures repeatability of the results. In order to truly randomize the noise acting on the outputs and also to incorporate the effect of noise in the surrogate model, we consider an additional uncertainty, which gives the seed values used by the random number generators in MATLAB to generate random noise signals in the original launcher model. This increases the total number of uncertainties considered to 29. The cost function is the performance specification against which the controller is validated. The entire list of cost functions is given in Table 2. Second-order polynomial models are generated for each of the cost functions. For a second-order model, the number of coefficients of the polynomial model is 465 (refer to Eq. 10). For each of the cost functions, 465 collocation points are generated and the flexible launcher model is evaluated at these points. These collocation points are common to all of the cost functions and, hence, all polynomials can be modeled by evaluating the original model just 465 times. A set of linear equations can be formed by substituting these collocation points and their corresponding output responses in Eq. 10. The coefficients of the polynomial are obtained by solving these set equations. comparison between the polynomial model and the original model is

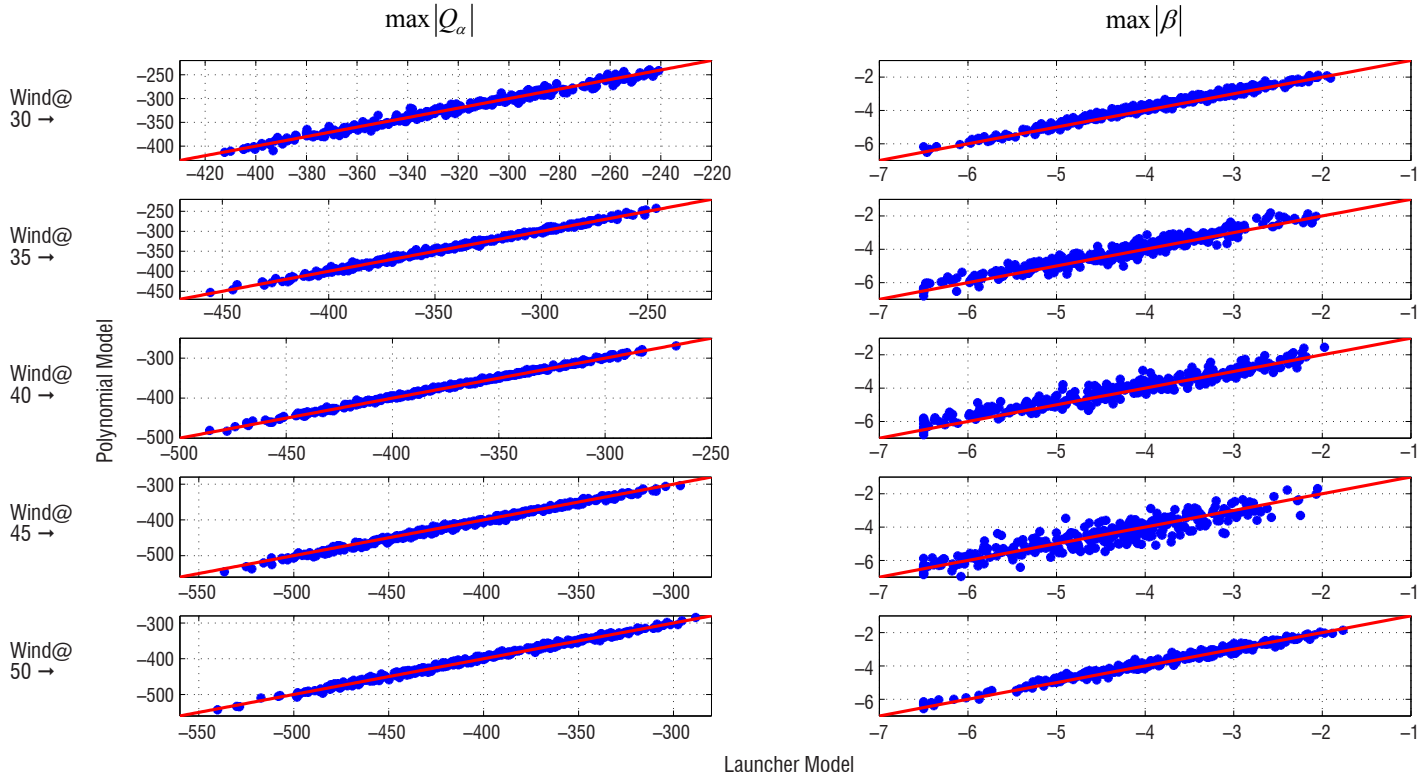

Figure 4 – Comparison between the launcher and polynomial models

shown in Figure 4. The comparison is shown for two performance criteria (along each column) at five different wind perturbations (along each row), which indicates a very good approximation.

Evolutionary-Based optimization: Hybrid Differential Evolution

The Differential Evolution (DE) method was first introduced by Storn and Price in [43] and is based on evolutionary principles. This method, like GA, starts with a random initial population. A new search point is generated by adding the weighted vector difference between two randomly selected individuals from the population with a third randomly chosen individual. The vector difference determines the search direction and a weighting factor decides the step size in that particular search direction. HDE employs a local optimization when no improvement is found from DE in successive iterations. Hybrid Differential Evolution (HDE) is used for optimization-based analysis in this paper. The results obtained by DE have been observed to be better than those of other evolutionary algorithms, both in terms of accuracy and computational overhead [44]. Please refer to [16, 17, 45] and the references therein for the HDE algorithm and its implementation.

Main Results

This section presents the results used to determine the efficacy of the controller. As a first step, a safety margin is evaluated and a comparison is made between the original launcher model and the polynomial model. The second step is to perform a worst-case analysis inside the safe region defined by the safety margin metric evaluated using the polynomial model. No constraint violations were found, thus indicating that the region defined by the metric is truly safe. Furthermore, a worst-case analysis is performed over the entire parameter space to gain insight into the level of performance deviations that could occur.

Results: Safety margin assessment

The safety margins for the given set of control laws $\mathcal{C}_{H_\infty}$ at five different wind perturbations occurring at 30, 35, 40, 45 and 50 seconds are determined by solving the constrained optimization in Eq. 8. A population-based optimization technique, specifically a Hybrid Differential Evolution (HDE) method, has been used to solve for the critical parameter values and the safety margins over the $\delta-$ space satisfying the performance requirements listed in Table 2. The critical similitude ratio ($\tilde{\lambda}$) and the safety margin (ρ) are evaluated for different wind perturbation cases, using a flexible launcher and polynomial model, and are given in Table 4. A high computation time, *i.e.*, more than 5 hours, is required to evaluate the parametric safety margin for each wind instance when the flexible launcher model is utilized.

		Wind perturbations				
		30 sec	35 sec	40 sec	45 sec	50 sec
Launcher Model	$\tilde{\lambda}$	1.05	0.71	0.66	0.68	0.88
	$\rho \geq 2.65$	2.78	1.88	1.75	1.8	2.32
	CPU Time (sec)	20914.33	16524.17	16948.07	18085.58	18381.9
Polynomial Model	$\tilde{\lambda}$	1.05	0.756	0.685	0.718	0.899
	$\rho \geq 2.65$	2.78	2	1.81	1.9	2.38
	CPU Time (sec)	181.27	442.16	211.41	366.65	204.07

Table 4 – Critical similitude ratio ($\tilde{\lambda}$) and safety margin (ρ) results for the launcher & the polynomial models

In order to reduce the computational time, surrogate polynomial models are utilized as constraints. It can be seen from Table 4 that the computational time is significantly reduced, by a factor of 100,

when the surrogate models are utilized. Due to the inherent error in the approximation, the critical parameter value found using the polynomial model is not the same as that found using the original launcher model.

It is found that $\tilde{\lambda} < 1$ for the wind perturbations occurring at 35, 40, 45 and 50 seconds. This indicates a reduced level of robustness, whereas for the wind perturbation occurring at 30 s, the value of λ is slightly greater than 1, indicating good robustness. For wind perturbations occurring at 40 and 45 seconds, the critical similitude ratio ($\tilde{\lambda}$) is 0.66 and 0.68 (for the launcher model), respectively, indicating that the reference set has contracted to a small safe region around the nominal parameter value.

Worst-case analysis inside the safe region

The worst-case analysis is carried out at five different wind perturbations occurring at 30, 35, 40, 45 and 50 seconds. The hybrid differential evolution is employed with a fixed termination criteria of 1200 simulations, a population size of 50, a mutation scale factor of 0.8 and a crossover factor of 0.8. The local optimization, sequential quadratic optimization "*fmincon*", is used for the hybridization purpose, and the maximum local iteration number is set to 30.

A worst-case analysis is performed on the original launcher model, in order to gain further insight about the levels of each performance deviation that could occur within the safe region defined by the parametric safety margin. In each case, the perturbations are limited within the set defined by the values of the parametric safety margin given in Table 4 respectively. Optimization-based worst-case analysis is performed for the cost functions listed in Table 2. The parameter space is restricted to be within the reference set defined by $\mathcal{R}(\delta_0, \tilde{\lambda}\mathbf{m})$, where $\mathbf{m}$ was kept fixed at 0.5 and $\tilde{\lambda}$ at the value from Table 4. The results of the worst-case analysis are shown in Table 5. None of the performance criteria were exceeded as expected and the maximum excursions for the performance requirements within the safe region are obtained. It is clear that the deflection angle performance requirement approached its limits and it is the first constraint violation in all of the cases.

Worst-case analysis over the entire parameter space

The numerical results for six different cost functions at five different wind perturbations are given in Table 6 - Table 7. In Table 6, consider the cost function representing the performance on the aerodynamic load $|Q(\alpha(t))|$ and wind occurring at 45 seconds. Among the 1200 candidate uncertain parameter vectors in the search space, the maximum cost function value associated with the worst case is 561.91 and has a mean of 436.11, with a standard deviation of 79.57. Mean and standard deviation statistics give us an idea of the variability of the cost function values in the search space. A high value of the standard deviation indicates that the cost function values are spread out over a large range in the search space, whereas a low value indicates that the cost function values lie too close to the mean. This shows the exploration property of the optimization algorithm, which is its ability to access uncertain parameter vectors spread out in the search space. In order to find the global solution, the optimization algorithm should be able to explore the search space as thoroughly as possible. In this case, the standard deviation is high and indicates that the algorithm was able to access uncertain parameter vectors spread out over the search space. Also, among the candidate points, 383 cases out

Cost Function		Worst case values				
		30s	35s	40s	45s	50s
$\max_{t\in[t_0 t_f]}\lvert Q_\alpha(t)\rvert$	max	388.11	393.44	423.09	467.65	476.51
	mean	340.85	355.41	385.65	425.83	423.46
	std	42.84	37.24	39.71	44.25	47.84
	failures	0	0	0	0	0
$\max_{t\in[t_0 t_f]}\lvert\beta(t)\rvert$	max	5.78	5.85	5.94	5.91	5.993
	mean	4.10	4.62	4.84	4.76	4.45
	std	0.85	0.71	0.67	0.68	0.83
	failures	0	0	0	0	0
$\max_{t\in[t_0 t_f]}\lvert\theta(t)\rvert$	max	4.51	4.24	4.21	4.53	4.13
	mean	3.51	3.46	3.56	3.51	3.04
	std	0.58	0.44	0.45	0.52	0.5
	failures	0	0	0	0	0
$\max\lvert\theta(t_{tf})\rvert$	max	0.199	0.152	0.144	0.145	0.138
	mean	0.038	0.033	0.032	0.035	0.034
	std	0.026	0.026	0.024	0.030	0.025
	failures	0	0	0	0	0
$\max\lvert\dot{\theta}(t_{tf})\rvert$	max	0.477	0.465	0.456	0.568	0.385
	mean	0.124	0.119	0.118	0.134	0.121
	std	0.095	0.095	0.090	0.101	0.101
	failures	0	0	0	0	0
Cumulated deflection	max	136.15	138.19	135.54	137.95	135.44
	mean	125.43	125.92	125.76	124.95	124.57
	std	12.1	12.31	12.00	11.81	11.42
	failures	0	0	0	0	0

Table 5 – Worst-case results inside the safe region

Cost Function			Worst-case values				
			30s	35s	40s	45s	50s
$\max_{t\in[t_0 t_f]}\lvert Q_\alpha(t)\rvert$	HDE	max	432.23	460.61	509.65	561.91	543.23
		mean	336.68	369.56	406.95	436.11	430.48
		std	62.53	66.12	75.46	79.57	77.49
		failures	0	0	37	383	370
	MC	max	424.74	449.14	493.08	549.26	532.14
		mean	319.58	340.42	376.16	411.67	402.38
		std	41.6	46.62	50.13	53.76	54.26
		failures	0	0	0	60	40
$\max_{t\in[t_0 t_f]}\lvert\beta(t)\rvert$	HDE	max	6.5	6.5	6.5	6.5	6.5
		mean	4.29	4.72	4.27	4.86	4.43
		std	1.32	1.38	1.44	1.35	1.38
		failures	187	516	582	517	366
	MC	max	6.47	6.5	6.5	6.5	6.5
		mean	3.79	4.26	4.36	4.4	3.88
		std	0.95	1.05	1.08	1.12	1.01
		failures	13	67	93	111	29
$\max_{t\in[t_0 t_f]}\lvert\theta(t)\rvert$	HDE	max	5.85	Unstable	Unstable	Unstable	6.91
		mean	3.51				3.41
		std	0.87				1.12
		failures	0				0
	MC	max	4.65	7.03	8.8	8.2	5.54
		mean	3.14	3.24	3.35	3.34	2.73
		std	0.59	0.7	0.76	0.95	0.63
		failures	0	0	0	0	0

Table 6 – Worst case results for entire parameter range

of 1200 violated the performance requirement on $Q(\alpha(t)) \leq 500$ kPa during the execution of the HDE optimization algorithm. It was noticed that the rigid uncertain parameters were the main cause for the worst-case performance in all of the cases, and the flexible modes were well suppressed by the bending-mode filters. Worst-case directions are oriented towards the parameters, which are simultaneously the most influent ones (dynamic pressure MQ, aerodynamic coefficient Cz, center of pressure Xf, center of gravity Xg) and the more dispersed ones (deflection misalignment).

Unstable cases are found for attitude when the wind perturbation corresponds to 35, 40, and 45 seconds. Sustained actuator saturation is observed in these cases. Monte Carlo analysis is also performed and the results are also tabulated in Table 6 - Table 7. These results are provided to compare with those found by optimization-based analysis. Due to the computational complexity involved with the original launcher model, 1000 Monte Carlo campaigns were performed for each cost function. It was observed that the optimization-based method is able to find more worst-cases and even better ones than those found by the Monte Carlo method, which can be attributed to the intelligence embedded in the search process of the optimization scheme. The Monte Carlo method is unable to capture any unstable cases corresponding to the performance criteria of attitude, attitude rate and cumulated deflection. Also, apart from Q_α and $\beta(t)$, no failures, *i.e.*, performance criteria violations, were recorded.

Cost Function			Worst case values				
			30s	35s	40s	45s	50s
$\max\lvert\theta(t_{tf})\rvert$	HDE	max	0.15	0.16	Unstable	Unstable	0.139
		mean	0.038	0.035			0.04
		std	0.027	0.029			0.03
		failures	0	0			0
	MC	max	0.22	0.18	0.19	0.184	0.177
		mean	0.04	0.04	0.04	0.04	0.04
		std	0.03	0.03	0.03	0.03	0.03
		failures	0	0	0	0	0
$\max\lvert\dot{\theta}(t_{tf})\rvert$	HDE	max	0.595	0.498	Unstable	Unstable	0.493
		mean	0.117	0.138			0.112
		std	0.09	0.101			0.088
		failures	0	0			0
	MC	max	0.556	0.54	0.53	0.58	0.536
		mean	0.13	0.13	0.13	0.13	0.122
		std	0.1	0.09	0.1	0.1	0.09
		failures	0	0	0	0	0
Cumulated Deflection	HDE	max	136.44	153.7	Unstable	Unstable	141.64
		mean	125.87	127.28			125.43
		std	14.05	13.55			12.85
		failures	0	0			0
	MC	max	136.52	142.51	151.14	142.18	135.63
		mean	126.81	127.3	127	127	126.36
		std	3.07	3.5	3.5	3.43	3.07
		failures	0	0	0	0	0

Table 7 – Worst-case results for the entire parameter range

Conclusion and future work

Parametric safety margin assessment provides means to quantify robustness in the parameter space. The methodology involves translating the performance criteria into constraints, which are used in an optimization problem. This optimization problem is formulated in such a way that dilations of the reference set are performed in order to find the largest hyper-rectangle in the parameter space around the nominal parameter value where all of the performance criteria/constraints are satisfied. This procedure involves a large number of simulations of the launch vehicle and the problem becomes computationally very expensive.

In order to reduce the computational burden, surrogate polynomial models were developed using the polynomial chaos theory. These models provided a relatively inexpensive way of calculating the operational parametric safety margin metric. Although polynomial models are computationally very cheap to utilize, they may be less accurate when compared with the original launcher model. The accuracy depends on the order of the polynomial. As the order is increased, the accuracy increases while significantly increasing the computation time to derive the polynomial models. Even so, this paper shows that the second order polynomial models could be used to generate results with a fair degree of accuracy.

Future work is aimed at investigating the method of Bernstein expansion on polynomial models to determine the parametric safety margin. The method of Bernstein expansion could further reduce the evaluation time of the safety margin by eliminating the use of the optimization procedure [46]; however, a stumbling block that needs to be overcome are the issues emanating from the dimensionality of the uncertainty space ■

References

[1] C. FIELDING, A. VARGA, S. BENNANI, M. SELIER - *Advanced Techniques for Clearance of Flight Control Laws*. Lecture Notes in Control and Information Sciences, Springer, 2002.

[2] R. W. PRATT, ED. - *Flight Control Systems.* Progress in Astronautics and Aeronautics, American Institute of Aeronautics and Astronautics, 2000.

[3] Y. JEPPU, K. KUNDAPUR, P. APTE - *Optimized Flight Control Component Testing Using Taguchi Design of Experiments*. American Institute of Aeronautics and Astronautics, 2014/11/19 2007. [Online]. Available: http://dx.doi.org/10.2514/6.2007-7824.

[4] A. PATEL, V. PATEL, G. DEODHARE, S. CHETTY - *Flight Control System Clearance Using Static Tests at Iron Bird*. American Institute of Aeronautics and Astronautics, 2014/11/19 2006. [Online]. Available: http://dx.doi.org/10.2514/6.2006-6203.

[5] V. PATEL, G. DEODHARE, S. CHETTY - *Near Real Time Stability Margin Estimation from Piloted 3-2-1-1 Inputs*. American Institute of Aeronautics and Astronautics, 2014/11/19 2002. [Online]. Available: http://dx.doi.org/10.2514/6.2002-5820.

[6] J. M. MACIEJOWSKI - *Multivariable Feedback Design*. Addison-Wesley, 1989.

[7] M. H. LOWENBERG - *Stability and Controllability Evaluation of Sustained Flight Manoeuvres*. Proceedings of 21st Atmospheric Flight Mechanics Conference. AIAA 1996-3422, July 1996.

[8] J. F. MAGNI - *Linear Fractional Representation Toolbox: Modelling, Order Reduction, Gain Scheduling*. System Control and Flight Dynamics Department, Onera, Toulouse, France, Tech. Rep., 2004.

[9] A. VARGA, A. HANSSON, G. PUYOU - *Optimization Based Clearance of Flight Control Laws: A Civil Aircraft Application*. Lecture Notes in Control and Information Sciences. Springer, 2011.

[10] R. P. BRAATZ, P. M. YOUNG, J. C. DOYLE, M. MORARI - *Compulational Complexity of μ Calculation*. IEEE Transactions on Automatic Control, vol. 39, no. 5, pp. 1000-1001, 1994.

[11] C. ROOS, J.-M. BIANNIC - *A Detailed Comparative Analysis of all Practical Algorithms to Compute Lower Bounds on the Structured Singular Value*. Control Engineering Practice, vol. 44, pp. 219–230, 2015.

[12] A. MEGRETSKI, A. RANTZER - *System Analysis via Integral Quadratic Constraints.* IEEE Transactions on Automatic Control, vol. 42, no. 6, pp. 819-830, 1997.

[13] J. M. BIANNIC, C. ROOS, A. KNAUF - *Design and Robustness Analysis of Fighter Aircraft Flight Control Laws*. European Journal of Control, vol. 12, no. 1, pp. 71-85, 2006.

[14] K. KRISHNASWAMY, G. PAPAGEORGIOU, S. GLAVASKI, A. PAPACHRISTODOULOU - *Analysis of Aircraft Pitch Axis Stability Augmentation System Using Sum of Squares Optimization*. Proceedings of American Control Conference, vol. 3, 2005, pp. 1497-1502.

[15] H. D. JOOS - *Flight Control Law Clearance Using Optimisation-Based Worst-Case Search*. Proceedings of 6th IFAC Symposium on Robust Control Design, vol. 6, no. 1, 2009, pp. 331-336.

[16] P. P. MENON, D. G. BATES, I. POSTLETHWAITE - *Nonlinear Robustness Analysis of Flight Control Laws for Highly Augmented Aircraft*. Control Engineering Practice, vol. 15, no. 6, pp. 655-662, 2007.

[17] P. P. MENON, I. POSTLETHWAITE, S. BENNANI, A. MARCOS, D. G. BATES - *Robustness Analysis of a Reusable Launch Vehicle Flight Control Law*. Control Engineering Practice, vol. 17, no. 7, pp. 751-765, 2009.

[18] L. G. CRESPO, D. P. GIESY, S. P. KENNY - *Robustness Analysis and Robust Design of Uncertain Systems*. AIAA Journal, vol. 46, pp. 388-396, 2008.

[19] H. S. CHUNG, J. J. ALONSO - *Comparison of Approximation Models with Merit Functions for Design Optimization*. Proceedings of 8th Symposium on Multidisciplinary Analysis and Optimization, vol. 200, AIAA 2000-4754, September 2000.

[20] R. JIN, W. CHEN, T. W. SIMPSON - *Comparative Studies of Metamodelling Techniques under Multiple Modeling Criteria*. Structural and Multidisciplinary Optimization, Springer-Verlag, vol. 23, no. 1, pp. 1-13, 2001.

[21] A. KHURI, S. MUKHOPADHYAY - *Response Surface Methodology*. Wiley Interdisciplinary Reviews: Computational Statistics, vol. 2, no. 2, pp. 128-149, 2010.

[22] J. P. C. KLEIJNEN - *Kriging Metamodeling in Simulation: A Review*. European Journal of Operational Research, vol. 192, no. 3, pp. 707-716, 2009.

[23] B. CHENG, D. M. TITTERINGTON - *Neural Networks: A Review from a Statistical Perspective*. Statistical Science, vol. 9, no. 1, pp. 2-30, 1994.

[24] M. GANET-SCHOELLER, M. DUCAMP - *LPV Control for Flexible Launcher*. Proceedings of AIAA Guidance, Navigation, and Control Conference. AIAA 2010-8193, 2010.

[25] M. GANET-SCHOELLER, J. BOURDON, G. GELLY - *Non-Linear and Robust Stability Analysis for ATV Rendezvous Control*. Proceedings of AIAA Guidance, Navigation, and Control Conference, AIAA 2009-5951, 2009.

[26] D. L. JOHNSON - *Terrestrial Environment (Climatic) - Criteria Guidelines for Use in Aerospace Vehicle Development*. NASA Technical Memorandum 4511, Revision, 1993.

[27] I. RONGIER, J. DROZ - *Robustness of Ariane 5 GNC Algorithms*. Proceedings of the 4th ESA International Conference on Spacecraft Guidance, Navigation and Control Systems, ESTEC, Noordwijk, The Netherlands, October, 1999.

[28] L. G. CRESPO, M. MATSUTANI, J. JANG, T. GIBSON, A. ANNASWAMY - *Design and Verification of an Adaptive Controller for the Generic Transport Model*. Proceedings of AIAA Guidance, Navigation, and Control Conference, AIAA 2009-5618, 2009.

[29] A. K. KAMATH, P. P. MENON, M. GANET-SCHOELLER, G. MAURICE, S. BENNANI, D. G. BATES - *Robust Safety Margin Assessment and Constrained Worst-Case Analysis of a Launcher Vehicle*. Proceedings of 7th IFAC Symposium on Robust Control Design, vol. 7, no. 1, 2012, pp. 254-259.

[30] R. GHANEM, J. RED-HORSE - *Propagation of Probabilistic Uncertainty in Complex Physical Systems Using a Stochastic Finite Element Approach*. Physica D: Nonlinear Phenomena, vol. 133, pp. 137-144, 1999.

[31] R. GHANEM - *Ingredients for a General Purpose Stochastic Finite Elements Implementation*. Computer Methods in Applied Mechanics and Engineering, vol. 168, no. 1, pp. 19-34, 1999.

[32] R. GHANEM, P. D. SPANOS - *Stochastic Finite Elements: A Spectral Approach*. Dover Publications, 2003.

[33] T. Y. HOU, W. LUO, B. ROZOVSKII, H. M. ZHOU - *Wiener Chaos Expansions and Numerical Solutions of Randomly Forced Equations of Fluid Mechanics*. Journal of Computational Physics, vol. 216, no. 2, pp. 687-706, 2006.

[34] D. XIU, G. E. KARNIADAKIS - *Modeling Uncertainty in Flow Simulations via Generalized Polynomial Chaos*. Journal of Computational Physics, vol. 187, no. 1, pp. 137-167, 2003.

[35] Z. K. NAGY, R. D. BRAATZ - *Distributional Uncertainty Analysis Using Polynomial Chaos Expansions*. Proceedings of IEEE International Symposium on Computer-Aided Control System Design, 2010, pp. 1103-1108.

[36] F. S. HOVER, M. S. TRIANTAFYLLOU - *Application of Polynomial Chaos in Stability and Control.* Automatica, vol. 42, no. 5, pp. 789-795, 2006.

[37] T. SINGH, P. SINGLA, U. KONDA - *Polynomial Chaos Based Design of Robust Input Shapers*. Journal of dynamic systems, measurement, and control, vol. 132, no. 5, 2010.

[38] J. FISHER, R. BHATTACHARYA - *Linear Quadratic Regulation of Systems with Stochastic Parameter Uncertainties*. Automatica, vol. 45, no. 12, pp. 2831-2841, 2009.

[39] D. XIU, G. KARNIADAKIS - *The Wiener-askey Polynomial Chaos for Stochastic Differential Equations*. SIAM Journal on Scientific Computing, vol. 24, no. 2, pp. 619-644, 2002.

[40] N. WIENER - *The Homogeneous Chaos.* American Journal of Mathematics, vol. 60, no. 4, pp. 897-936, 1938.

[41] M. D. WEBSTER, M. A. TATANF, G. J. MCRAE - *Application of the Probabilistic Collocation Method for an Uncertainty Analysis of a Simple Ocean Model*. Tech. Rep. 4, 1996.

[42] A. K. KAMATH, P. P. MENON, M. GANET-SCHOELLER, G. MAURICE, S. BENNANI, D. G. BATES - *Worst Case Analysis of a Launcher Vehicle Using Surrogate Models.* Proceedings of 7th IFAC Symposium on Robust Control Design, vol. 7, no. 1, 2012, pp. 260-265.

[43] R. STORN, K. PRICE - *Differential Evolution – A Simple and Efficient Heuristic for Global Optimization Over Continuous Spaces*. Journal of Global Optimization, vol. 11, no. 4, pp. 341-359, 1997.

[44] P. P. MENON, D. G. BATES, I. POSTLETHWAITE - *Hybrid Evolutionary Optimisation Methods for the Clearance of Nonlinear Flight Control Laws*. 44th IEEE Conference on Decision and Control, European Control Conference. CDC-ECC '05., December 2005, pp. 4053-4058.

[45] W. WANG, P. P. MENON, D. G. BATES, S. BENNANI - *Robustness Analysis of Attitude and Orbit Control Systems for Flexible Satellites*. Control Theory Applications, IET, vol. 4, no. 12, pp. 2958-2970, December.

[46] M. ZETTLER, J. GARLOFF - *Robustness Analysis of Polynomials with Polynomial Parameter Dependency Using Bernstein Expansion.* IEEE Transactions on Automatic Control, vol. 43, no. 3, pp. 425-431, 1998.

AUTHORS

Atul Kamath received the B.Eng. degree in electrical from Mumbai University, Mumbai, India, in 2005, the M.Tech. degree in control system engineering from Mumbai University, Mumbai, India., in 2008, and the Ph.D. degree in control engineering from the University of Exeter, Exeter, U.K., in 2014. He is currently working with General Electric's Global Research Center, Bangalore, India as a control system engineer. Email address: atul.kamath@ge.com

Prathyush P Menon is a senior lecturer in Mathematics. His research interests are control, optimisation, robustness analysis and autonomy.

Martine Ganet-Schoeller is currently a flight control engineer at Ariane Group in Les Mureaux, France.

Guillaume Maurice received a Master degree in engineering from ISAE Supaero, France in 2010. He is currently a flight control engineer at Ariane Group in Les Mureaux, France.

Samir Bennani has obtained a M.Sc. and a Ph.D from the TU Delft in aerospace engineering with specialisation in the field of systems theory and robust control applied to flight control systems. He is Guidance Navigation & Control System Engineer at European Space Agency (ESA), ESTEC. Within ESA, Samir Bennani has obtained the highest merit recognition in the field on Control being recommend as Ad Personal Control Systems Engineer to shape future needs and Competence Domain Lead Engineer for Space Transportation, Re-entry and Propulsion. He is a senior member of various international professional associations including the AIAA, IFAC and IEEE control systems society.